were used. Error-rate measurements made over the 102 km of monomode fibre were compared with back-to-back measurements made over the 1 m fibre tail of the transmitter module. In order that this could be done easily, micromanipulated butt-coupled joints were made between the fibre tail of the transmitter module, the transmission fibre and the graded-index fibre tail of the receiver module. Index matching gel was placed between the fibre ends to reduce reflection losses and to avoid the possibility of reflections affecting the laser. The received power was varied to plot error-rate curves by misaligning the joint to the fibre tail of the receiver module.

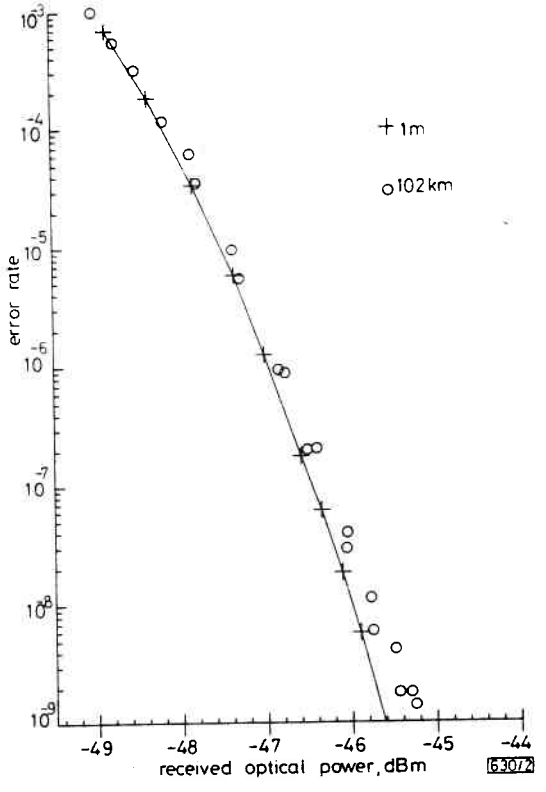

Fig. 2 *Error-rate curves*

Fig. 2 shows the results of error-rate measurements made back-to-back without the external cavity and over 102 km with the cavity fitted and tuned for single longitudinal mode operation of the laser. The received powers required a bit-error rate of 10^{-9} differ by less than 0·5 dB. In contrast, when the transmitter module was operated over 102 km prior to the fitting of the reflector it was not possible to obtain an error rate lower than 10^{-4} even at the maximum received power of −42 dBm. Equalised eye diagrams after 102 km with and without the reflector in place are shown in Fig. 3. The system margin with the external cavity was greater than 3 dB after 102 km.

In conclusion, we have demonstrated that the degree of spectral control achieved in an external cavity controlled transmitter module was sufficient to allow 140 Mbit/s oper-

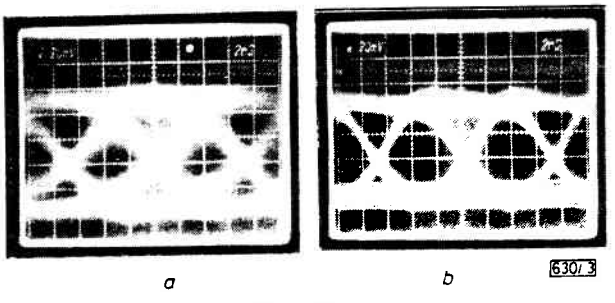

Fig. 3 *Eye diagrams over 102 km fibre*

a No external cavity
b With external cavity

Acknowledgments: We wish to thank colleagues at BTRL who have contributed to this work and the Director of Research of British Telecommunications for permission to publish this letter.

K. H. CAMERON
P. J. CHIDGEY
K. R. PRESTON

British Telecom Research Laboratories
Martlesham Heath, Ipswich, Suffolk IP5 7RE, England

14th June 1982

References

1 BERKEY, G. E., and SARKAR, A.: 'Single-mode fibers by the OVD process'. Topical meeting on optical fiber communication, Phoenix, Arizona, 13–15 April 1982
2 AINSLIE, B. J., BEALES, K. J., DAY, C. R., and RUSH, J. D.: 'The reproducible fabrication of ultra low loss single fibre'. 7th European Conference on optical communications, Copenhagen, 1981
3 COHEN, L. G., LIN, CHINLON, and FRENCH, W. G.: 'Tailoring zero chromatic dispersion into the 1·5–1·6 μm low-loss spectral region of single mode fibres', *Electron. Lett.*, 1979, **15**, pp. 334–335
4 YAMADA, J., KAWANA, A., NAGAI, H., and KIMURA, T.: '1·55 μm optical transmission experiments at 2 Gbit/s using 51·5 km dispersion-free fibre', *ibid.*, 1982, **18**, pp. 98–100
5 YAMAMOTO, S., UTAKA, K., AKIBA, S., SAKAI, K., MATSUSHIMA, Y., SAKAGUCHI, S., and SEKI, N.: '280 Mbit/s single-mode fibre transmission with DFB laser diode emitting at 1·53 μm', *ibid.*, 1982, **18**, pp. 239–240
6 MALYON, D. J., and MCDONNA, A. P.: 'A 102 km unrepeatered monomode fibre system experiment at 140 Mbit/s with an injection locked 1·52 μm laser transmitter', *ibid.*, 1982, **18**, pp. 445–447
7 PRESTON, K. R., WOOLLARD, K. C., and CAMERON, K. H.: 'An external cavity controlled single longitudinal mode laser transmitter module', *ibid.*, 1981, **17**, pp. 931–933
8 CAMERON, K. H., CHIDGEY, P. J., PRESTON, K. R., SMITH, D. W., and MATTHEWS, M. R.: 'A laser transmitter module for monomode fibre transmission systems'. Paper presented at IEE Colloquium on optical fibre systems, London, 29 May 1981
9 SMITH, D. R., HOOPER, R. C., SMYTH, P. P., and WAKE, D.: 'Experimental comparison of a germanium avalanche photodiode and InGaAs PINFET receiver for longer wavelength optical communication systems', *Electron. Lett.*, 1982, **18**, pp. 453–454

0013-5194/82/150650-02$1.50/0

THERMAL WAVE IMAGING THROUGH RADIO FREQUENCY INDUCTION HEATING

Indexing terms: Acousto-optics, Thermal imaging

Radio frequency (RF) induction heating is used in order to generate thermal waves in conducting materials. This technique is applied to measure the thickness of tungsten-carbide plasma coating on stainless-steel plates. The letter briefly discusses major advantages and disadvantages of RF induction heating.

The photothermal or photoacoustic characterisation of materials has been demonstrated to have great potential in the field of nondestructive testing.[1] In these studies, thermal waves are generated by an optical source or by an electron microscope even though other means of thermal wave generation can be of practical interest. A provocative alternative technique is RF induction heating whose history can be traced back to over a century ago. When a conductor is subjected to an alternating magnetic field, an electric current will be induced in the conductor. If the conductivity is high and the

frequency is high, the current tends to concentrate toward the outside of the conductor, resulting in surface or near-surface heating.

The experimental block diagram of RF induction heating is presented in Fig. 1. The modulated RF signal is amplified and fed into the coil. The energy is then induced in the sample and the thermal waves generated are diffused and become detected by an infra-red (IR) sensor. The existing delay between the modulated input energy and the detected signal is informative in characterising the sample. Under ideal conditions, this delay is linearly related to the thickness of the sample, and the delay can be measured by a lock-in analyser. One may use the amplitude or heating and cooling pattern for the characterisation of the specimen.

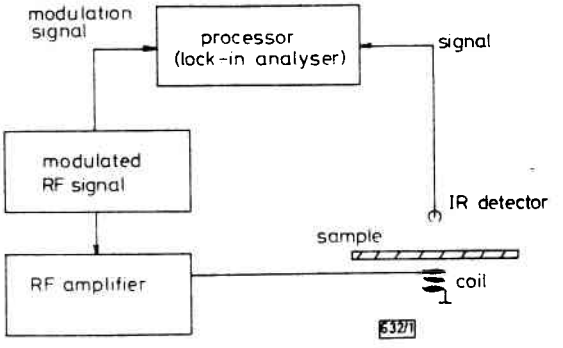

Fig. 1 *Experimental block diagram of thermal wave imaging of a sample through RF induction heating*

The induced current[2] $i(x, y, z; t)$ is the source of heating in the conducting sample, and this current decreases exponentially as a function of depth z such that

$$i(x, y, z; t) = i_0(x, y)e^{-z/\delta}e^{j(wt - z/\delta)}$$

$$\delta = \frac{2}{w\mu_r \mu_0 \sigma}$$

where the quantity δ is called the depth of penetration or skin depth, the constant σ is the conductivity of the conductor, w is the angular frequency of the RF signal, μ_0 is the permeability of vacuum $= 4\pi \times 10^{-7}$ Hm^{-1}, and μ_r is the relative permeability of the conducting sample. The term $i_0(x, y)$ is the amplitude of the current density on the surface of the conductor and it can very according to the position of the surface relative to the inducting coil and its geometry. Nevertheless, when the distance between the coil and the conductor is very small, the distribution of the surface current is approximately uniform under the coil and decreases significantly as the relative distance increases. As one can see from the above equation, the current is distributed in the outer layer of the conducting sample and the thickness of this layer is confined to skin depth. For example, at room temperature and $w = 2\pi \times 15 \times 10^6$ rad/s, the skin depth in aluminium and stainless-steel samples are approximately 25 and 110 μm, respectively. In practice, when examining samples of the order of a millimetre, it is reasonable to assume that the input energy produced through RF induction is concentrated on the surface.

The thickness measurement of plasma coating and the non-destructive evaluation (NDE) of the bonding between the coating and the substrate (test of the integrity) is highly desirable. In order to demonstrate the potential of RF heating for the characterisation of the materials, we have chosen tungsten-carbide plasma coating on stainless-steel plates of 1·33 mm thickness. The thicknesses of coating were 0·11, 0·20 and 0·30 mm. These samples are positioned as closely to the top of the coil as possible where the surface of the stainless steel is heated. The time delay or phase between the IR detected signal and the modulated input energy corresponds to the thicknesses of the stainless steel and the coating. Since the base metals (i.e. stainless-steel plates) are the same for all samples, the different phase angles of the samples correspond to the differences in the thicknesses of the coatings. Actually, we used the sample of 0·11 mm thickness as a reference and evaluated the phase change[3] $\Delta\phi$, due to the thickness change Δx, $\Delta\phi = (\pi f/\alpha)\,\Delta x$, where f is the modulation frequency and α is the thermal diffusivity governed by the thermal conductivity K, specific heat C_p and the mass density ρ [$\alpha = \sqrt{(K/\rho C_p)}$].

Experimental results for the modulation frequency of 1, 2, 3, ..., 10 Hz are shown in Fig. 2. From these results, it appears that the thickness of coating can be measured with resolution of the order of 10 μm. The resolution of measurement can be improved using higher modulation frequency. However, the sensitivity of the IR detector decreases significantly, and, in addition, the thermal wave becomes highly attenuated in the sample with increasing w, which results in poor signal/noise ratio and significantly decreases the accuracy of the measurement. We further used these results to evaluate the relationship between the phase and modulation frequency as discussed above. Using the best fit (least-square error), the phase is related to the modulation frequency by a power factor of 0·65 which differs slightly from the predicted or theoretical value of 0·5. This slight difference can be related to multiple factors such as insufficient signal/noise ratio, lack of surface heating due to skin depth, and possibily the inadequacy of a one-dimensional model of thermal diffusion wave which relates the phase lag to modulation frequency by a power factor of 0·5.

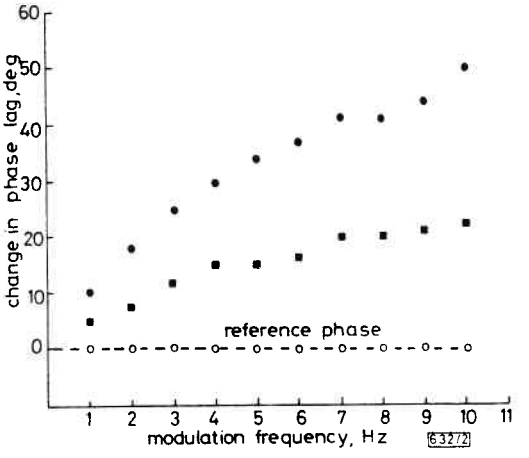

Fig. 2 *Change in phase lag against modulation frequency for tungsten-carbide plasma coating with thicknesses of 0·20 mm (■) and 0·30 mm (●) relative to coating with thickness of 0·11 mm (○)*

In the course of our investigation, RF induction heating has revealed several advantages and disadvantages which can be listed briefly as follows:

Advantages of RF induction heating:

(i) Input energy is easily adjusted by changing the coil geometry, the input power to the coil, or the distance between the coil and the conductor.
(ii) The depth of penetration of the input energy can be varied by changing the frequency of the RF signal.
(iii) RF heating can be done in a vacuum or at any practical temperature.
(iv) Modulation of the RF signal is electronically controllable and no practical limitations exist on the form of frequency of the modulation signal.
(v) The shape of the coil can be tailored to a particular application without much effort.
(vi) Subsurface features will contribute to RF input energy or will channel the induced current in a particular path which, if localised, can be quite useful in the characterisation of the sample.
(vii) RF heating of a conductor can also be performed through a dielectric, and the detected thermal waves can be used to evaluate the thermal properties of dielectric or its bonding with the conductor.
(viii) Testing of materials can be performed contactless.

Disadvantages of RF induction heating:

(i) In some instances, the RF signal may interfere with the IR detector or the processor.
(ii) The coil heats up as well as the sample, which may make it difficult to shield out its IR radiation.

(iii) The focusing of the RF field through the use of a different coil is limited. This focusing problem degrades the lateral resolution.
(iv) RF heating requires a conductor: however, nonconducting materials can be heated by adhering strips of conducting tape.

Acknowledgments: We wish to thank Martti Jokinen for his technical assistance and Funds for Finnish Independence (SITRA) for financial support.

J. SANIIE
M. LUUKKALA
A. LEHTO
R. RAJALA

14th June 1982

Department of Physics, University of Helsinki
Siltavuorenpenger 20 D, 00170 Helsinki 17, Finland

References

1 ASH, E. A. (Ed.): 'Scanned image microscopy' (Academic Press, London, 1980), pp. 247–364
2 RAMO, A., WHINNERY, J. R., and DUZER, T. V.: 'Fields and waves in communication and electronics' (Wiley & Sons, New York, 1967), pp. 249–254
3 HSU, S. T.: 'Engineering heat transfer' (D. Van Nostrand Co., New York, 1963), pp. 61–67

0013-5194/82/150651-03$1.50/0

CHARACTERISTICS OF ANODIC NATIVE OXIDE MIS DIODES OF $In_{0.53}Ga_{0.47}As$

Indexing terms: Semiconductor devices and materials, Oxides

Anodic native oxide has been formed on $In_{0.53}Ga_{0.47}As$ layers lattice-matched to InP substrate. Auger analysis of the oxide layers and capacitance/voltage characteristic measurements of MIS diodes are carried out. A U-shaped distribution of the density of surface states, the minimum of which is located at $E_c - 0.15$ eV and is about 2.2×10^{12} $cm^{-2}eV^{-1}$, is observed.

An $In_{0.53}Ga_{0.47}As$ layer lattice-matched to InP substrate has an electron mobility as high as 1.2×10^4 cm^2/Vs even at room temperature, implying its promising application to high-speed FETs and heterojunction bipolar transistors.[1] In order to realise $In_{0.53}Ga_{0.47}As$ FETs with high input impedance and wide dynamic range, a MIS structure is inevitable. Several attempts have native plasma oxides on *n*-type $In_{0.53}Ga_{0.47}As$ and estimated the density of surface states to be 3×10^{12} $cm^{-2}eV^{-1}$. They also observed the formation of the inversion layer on the surface of *p*-type $In_{0.53}Ga_{0.47}As$. Wieder *et al.*[3] made inversion-mode insulated-gate $In_{0.53}Ga_{0.47}As$ FETs using SiO_2 film deposited by a plasma CVD method. They reported a brief transistor characteristic, but no information on insulator/semiconductor interface states. $In_{0.53}Ga_{0.47}As/Si_3N_4$ *n*-channel inversion-mode MIS FET was reported by Liao *et al.*[4]

In this letter we describe anodic oxidation of *n*-type $In_{0.53}Ga_{0.47}As$, Auger analysis of the anodic native oxide and capacitance/voltage characteristics of MIS diodes along with some information on the surface state density.

Undoped $In_{0.53}Ga_{0.47}As$ layers were grown on semi-insulating InP substrate at 650°C by conventional LPE method. The typical thickness of $In_{0.53}Ga_{0.47}As$ layers was 5 μm. The density and mobility of electrons in ternary layers at room temperature ranged from 9×10^{15} to 3×10^{16} cm^{-3}

terned into a 3×3 mm^2 square by photolithography. The electrolyte employed was a standard one which has been developed for GaAs.[5] The electrolytic solution was a mixture of 3% aqueous solution of tartaric acid adjusted by ammonia water to be pH = 7 and propylene glycol in the volume ratio of 1:2. Prior to starting anodic oxidation, the surface of the epitaxial layer was lightly etched with a solution consisting of H_2O_2:10 and NH_4OH:1. The anodic oxidation was carried out at room temperature and the sample was placed in the dark during the oxidation. A constant voltage was applied to a circuit consisting of the electrolyte, an $In_{0.53}Ga_{0.47}As$ sample and a variable series resistor. The oxidation was started at a current density of 2.5 $\mu A/mm^2$ and was stopped at half the initial current density. Oxidised layers with a thickness of about 8000 Å were obtained by this procure.

The as-oxidised layers showed very poor electrical properties. However, after heat treatment in a flowing dry nitrogen at 250°C for 1–1.5 h, the quality of the oxide layers was much improved to a level enough to be used for measurements of the MIS characteristic. The oxide layers after the annealing showed a breakdown field higher than 1.7 MV/cm. Although the annealing condition was not optimised, the estimated breakdown field was somewhat higher than that reported for native plasma oxide (1 MV/cm).[2] From the capacitance/voltage measurement of MIS diodes, the static dielectric constant of the anodic native oxide was estimated to be about 7.5.

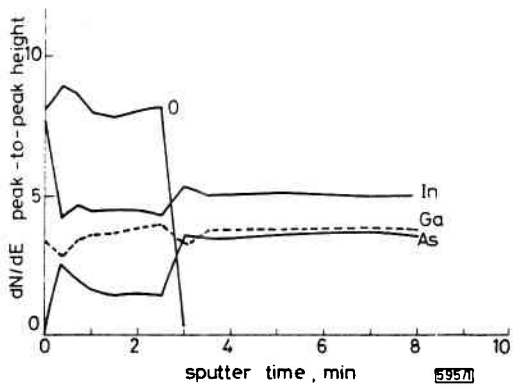

Fig. 1 *In-depth profile of In, Ga, As and O contents*

In order to investigate the compositional profile of the anodic oxide layer, an Auger analysis was performed. Fig. 1 shows the in-depth profile of the peak-to-peak height of the differentiated Auger spectrum for each element in a sample treated at 250°C for 1 h. 1 min of the sputter time corresponds to about 600 Å. The width of the transition region at the boundary between oxide and semiconductor is estimated to be less than 300 Å. The compositional in-depth profile of the elements did not change before and after the annealing as confirmed by Auger analysis; this is due to a low annealing temperature such as 250°C. The general features of the in-depth profile elucidated from the results on several samples are as follows:

(i) Indium has a tendency to accumulate at the oxide/semiconductor boundary and the oxide surface. The accumulation of In at the surface was reflected on the Auger spectrum of In in which the Auger peak at the surface was close to that in the $In_{0.53}Ga_{0.47}As$ epitaxial layer or that of metallic In.[6]
(ii) Gallium shows a small dip of the composition at the oxide/semiconductor boundary.
(iii) Arsenic composition depletes at the surface accompanying a pile-up on the inside of the surface.
(iv) Oxygen content decreases at the surface, being consistent with the existence of free indium and/or the depletion of arsenic.

From the Auger spectra measured at various in-depth positions, Ga and In atoms showed almost complete chemical bonding with oxygen to form Ga$_2$O$_3$ and In$_2$O$_3$ respectively